

# Synergistic surface current mapping by spaceborne stereo imaging and coastal HF radar

John Philip Matthews<sup>1</sup> and Yutaka Yoshikawa<sup>1</sup>

Received 2 June 2012; revised 4 August 2012; accepted 6 August 2012; published 15 September 2012.

[1] Well validated optical and radar methods of surface current measurement at high spatial resolution (nominally <100 m) from space can greatly advance our ability to monitor earth's oceans, coastal zones, lakes and rivers. With interest growing in optical along-track stereo techniques for surface current and wave motion determinations, questions of how to interpret such data and how to relate them to measurements made by better validated techniques arise. Here we make the first systematic appraisal of surface currents derived from along-track stereo Sun glitter (ATSSG) imagery through comparisons with simultaneous synoptic flows observed by coastal HF radars working at frequencies of 13.9 and 24.5 MHz, which return averaged currents within surface layers of roughly 1 m and 2 m depth respectively. At our Tsushima Strait (Japan) test site, we found that these two techniques provided largely compatible surface current patterns, with the main difference apparent in current strength. Within the northwest (southern) comparison region, the magnitudes of the ATSSG current vectors derived for 13 August 2006 were on average 22% (40%) higher than the corresponding vectors for the 1-m (2-m) depth radar. These results reflect near-surface vertical current structure, differences in the flow components sensed by the two techniques and disparities in instrumental performance. The vertical profile constructed here from ATSSG, HF radar and ADCP data is the first to resolve downwind drift in the upper 2 m of the open ocean. The profile e-folding depth suggests Stokes drift from waves of 10-m wavelength visible in the images. **Citation:** Matthews, J. P., and Y. Yoshikawa (2012), Synergistic surface current mapping by spaceborne stereo imaging and coastal HF radar, *Geophys. Res. Lett.*, 39, L17606, doi:10.1029/2012GL052546.

## 1. Introduction

[2] The measurement of currents from space represents an important means of tracking the transport of heat and nutrients in the world's oceans. Generally speaking, altimetric and gravimetric techniques working at low (say > 10 km) spatial resolutions can be used to carry out this task [e.g., Fu et al., 2010; Bingham et al., 2011] but a number of key aspects of ocean circulation, including flows through narrow sea straits, small-scale eddy morphology, sea-ice motion,

current convergence at fronts, the development of plankton patches and discharges at major estuaries require monitoring at considerably higher spatial resolutions. Flows in rivers and lakes likewise require a fine-scale spaceborne mapping capability, while recent oil pollution and tsunami-related catastrophes have also underscored the need for detailed synoptic current mapping by satellite.

[3] Several techniques, such as those based on active Synthetic Aperture Radar (SAR) [Goldstein and Zebker, 1987; Goldstein et al., 1994; Graber et al., 1996; Chapron et al., 2005; Liu and Hsu, 2009; Romeiser et al., 2010] or on inter-image feature tracking within passive image pairs [Steissberg et al., 2005; Turiel et al., 2008; Matthews and Emery, 2009; Kääh and Prowse, 2011] have the potential to deliver high resolution current measurements from space. However, these approaches will require rigorous and repeated validation of the type that is normally demanded of *in situ* and ground-based oceanographic instrumentation before they become widely accepted within the marine science community.

[4] We have recently determined surface currents using a promising optical tracking method termed the Along Track Stereo Sun Glitter (ATSSG) technique, which was first developed on the basis of data acquired at 15-m spatial resolution by the Advanced Spaceborne Thermal Emission and Reflection Radiometer (ASTER) [Matthews et al., 2004; Matthews, 2005] and then more recently applied at higher spatial resolution [Matthews and Awaji, 2010]. Our aim was to derive high spatial resolution surface currents in the Tsushima Strait of western Japan (Figure 1) and to compare these satellite-based flow determinations with simultaneous and better validated surface current data gathered by an extensive array of ground-based HF radars (Figure 1) maintained by the Research Institute for Applied Mechanics (RIAM) of Kyushu University, Japan [Yoshikawa et al., 2006; Yoshikawa et al., 2010]. This coastal system monitors the interchange between the Japan Sea and the warmer waters further south and offers long-term synoptic perspectives on the behavior of an important branch of the Kurushio termed the Tsushima Warm Current. In contrast to the deployment of single or paired HF radars in early oceanographic applications of the HF radar technique [e.g., Prandle and Matthews, 1990; Matthews et al., 1993], the installation of such extensive HF-radar coastal networks has become a feature of recent research [Yoshikawa et al., 2006; Kim et al., 2011].

## 2. Method

[5] The ATSSG technique employs Sun glitter images of water bodies that are separated in time by roughly one minute and are gathered in the forward-, nadir- and backward-looking directions by spaceborne sensors operating in along-track mode. As astronauts have often noted when looking

<sup>1</sup>Center for East Asian Ocean-Atmosphere Research, Research Institute for Applied Mechanics, Kyushu University, Kasuga, Japan.

Corresponding author: J. P. Matthews, Center for East Asian Ocean-Atmosphere Research, Research Institute for Applied Mechanics, Kyushu University, 6-1 Kasuga Park, Kasuga, Fukuoka, 816-8580, Japan. (johnp\_matthews@hotmail.com)

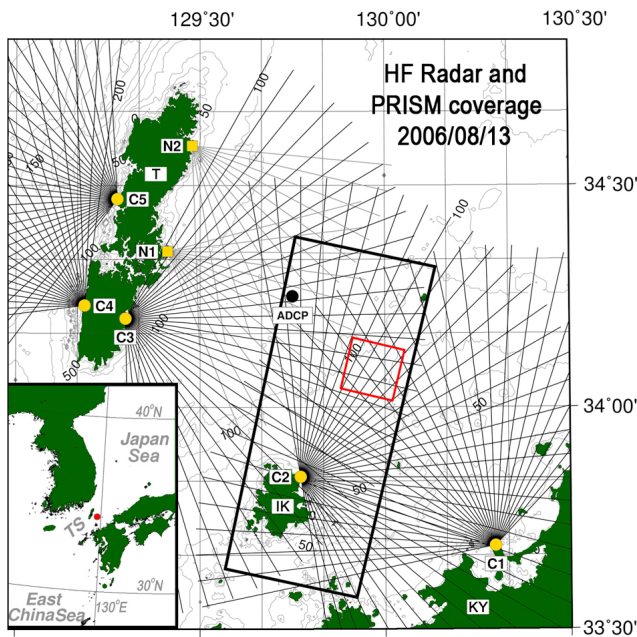


**Figure 1.** HF radar and PRISM coverage. T = Tsushima Island, IK = Iki Island, KY = Kyushu, C1 – C5 = CODAR HF radar sites, N1 – N2 = NJRC HF radar sites. ADCP = Acoustic Doppler Current Profiler mooring. Tilted black rectangle shows coverage from three consecutive PRISM stereo images acquired on 13 August 2006. Red box defines area covered in Figures 2a and 2b. Depth contours are given in meters. Inset: Tsushima Strait (TS), red dot indicates test area.

down on the earth [Munk *et al.*, 2000], Sun glitter is particularly effective at revealing ocean (or lake) surface structure, since the reflected glitter radiance is strongly affected by the presence of artificial slicks, organic films and a variety of aquatic phenomena such as internal waves, gravity waves, and frontal convergence. In tracking the motion of matching Sun glitter features between successive images within an along-track stereo “take”, the ATSSG technique makes use of this powerful highlighting capability. Note that in the absence of Sun glitter, the ocean would generally be imaged as a relatively dark, low-reflectivity region and the surface features that are prominent in the Sun glitter regime would then become difficult if not impossible to identify.

[6] The glitter images used in this study were gathered by the Panchromatic Remote-sensing Instrument for Stereo Mapping (PRISM), which operated on the Advanced Land Observing Satellite (ALOS) between January 2006 and April 2011. This instrument maps in panchromatic mode (520–770 nm) across a swath width of 35 km for stereo triplets in which the backward and forward slant views are tilted at  $\pm 24^\circ$  with respect to nadir. The time of separation between adjacent views within the stereo triplet is nominally 45.3 s, so that with a sensor spatial resolution of 2.5 m the speed resolution becomes nearly  $5.5 \text{ cm s}^{-1}$  in the case of good inter-image feature correspondence. The selection of appropriate images from the image database gathered by PRISM in our region of interest (Figure 1) requires some care since most data covering the ocean contain little or no Sun glitter, as can be expected from a mission whose goal lies in topographic mapping over land. For example, during 2006 we have identified only 10 workable triplet frames in this vicinity out

of a total of 66. These were gathered on relatively cloud-free days during the summer months when the observational geometry satisfied the requirements for Sun glitter imaging of water surfaces [Matthews, 2005].

[7] In a later section of the paper we have also made use of 90-m spatial resolution thermal infrared (TIR) imagery gathered by ASTER, although we have not considered any further ATSSG applications based on the stereo capability of the Visible and Near Infrared (VNIR) sensor of ASTER as the considerably higher spatial resolution of PRISM leads to a significant advance in ATSSG performance. Thermal infrared data gathered by the Moderate Resolution Imaging Spectroradiometer (MODIS) at 1-km spatial resolution have also been used to define surface temperature structures within our study region.

[8] The region of coverage of three consecutive PRISM stereo images collected over the eastern channel of the Tsushima Strait under calm conditions on 13 August 2006 at around 11.11 LT, when Sun glitter was best defined in the forward and nadir views, is depicted by the heavy rectangular box in Figure 1. Surface current determinations at radar beam intersection points are provided within this region by the RIAM network of coastal HF radar systems. The transmitter sites are labeled as C1, C2 and C3 for CODAR radars and N1 and N2 for radars supplied by the Nagano Japan Radio Company (NJRC) [Yoshikawa *et al.*, 2006]. Note that data from radars C4 and C5, which cover the western channel of the Tsushima Strait, are not used in this study. An Acoustic Doppler Current Profiler (ADCP) operated from a mooring site in the northern section of the PRISM coverage where the water depth is 107 m.

[9] Stereo images from a sub-region selected from the northern half of the PRISM coverage (red box of Figure 1) are shown in Figures 2a and 2b, respectively. Both of these Sun glitter views resemble SAR images in that they reveal ocean surface structure, with numerous slicks, internal waves and surface gravity waves clearly defined. The high speed jetfoil ferry linking the ports of Pusan (South Korea) and Hakata (Japan), which can be identified in the bottom right corners of Figures 2a and 2b, has been highlighted because it provides a means of checking the accuracy of the along-track stereo motion determinations. Measurement of the inter-image displacement of this vessel yields a speed of  $21.9 \text{ m s}^{-1}$  on a bearing of  $330^\circ$ , which compares favorably with the values logged by the jetfoil company (JR Kyushu Jet Ferry Inc.) of 41 knots ( $21.1 \text{ m s}^{-1}$ ) on  $332^\circ$  some 9 minutes after the time of the ALOS overpass. This correspondence, together with other evidence, supports our view that the inter-image co-registration, performed here using reference “tie-in” points located on Iki Island (IK) and other small islands, is satisfactory. By comparing the positions of many static sea-level features visible in both images, we estimate a representative co-registration error of 1 pixel, which translates into an uncertainty of about  $5.5 \text{ cm s}^{-1}$  in speed.

[10] We obtain a further, though less rigorous, reassurance of the accuracy of the motion determinations by measuring the inter-image displacement of cloud shadows on the sea surface, which are well defined in both views. This approach gives a cloud-height wind speed and direction near the ADCP mooring of  $3.9 \text{ m s}^{-1}$  and  $59.8^\circ$ , respectively, as compared with values at 10-m height of  $2.8 \text{ m s}^{-1}$  at  $62.3^\circ$  predicted near the time of the overpass by the Grid Point

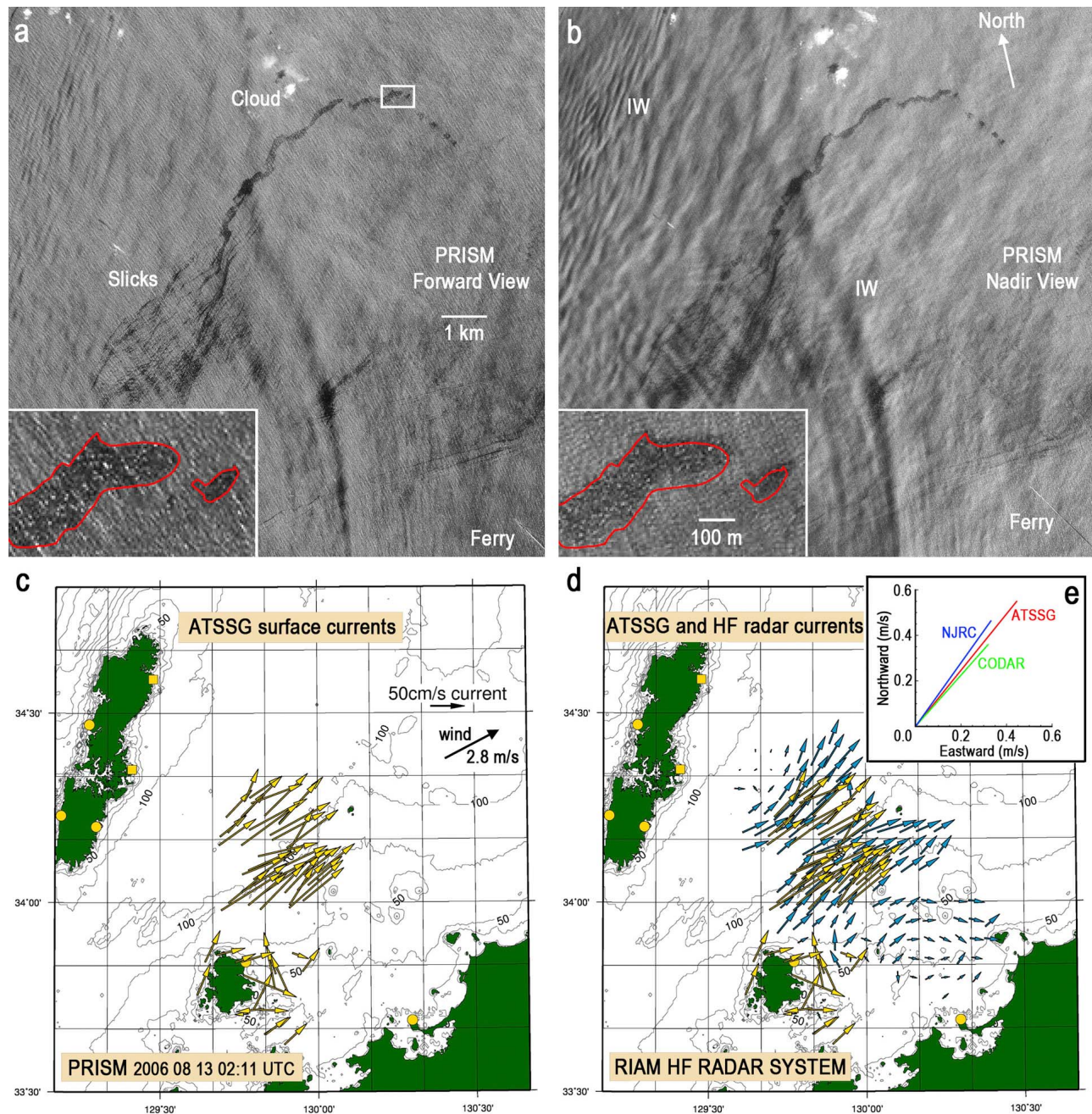


**Figure 2.** (a) PRISM Forward view with slick features contained in small white rectangle enlarged in the bottom left inset and outlined in red. (b) PRISM Nadir view acquired 45.2 s later, with inset depicting slick displacements, IW = internal waves. (c) ATSSG-derived surface currents. (d) ATSSG and HF radar-derived surface currents. The NJRC and CODAR data represent averages over 10.45–11.15 LT and 10.30–11.30 LT respectively. (e) Results of two complex Principal Component analyses performed for paired ATSSG and HF radar current determinations within the NJRC and CODAR regions of coverage, respectively. Here the first mode vectors are displayed. Both ATSSG first modes have been scaled to the magnitude and direction of the overall mean ATSSG surface current.

Value – MesoScale Model (GPV-MSM) dataset of the Japan Meteorological Agency.

[11] The required surface currents are similarly deduced from visual comparison of the forward and nadir views by measuring the differential displacements of many matching surface slick features visible in both images and then computing current velocities. The technique is illustrated in the

insets at the bottom of Figures 2a and 2b, which represent zoomed versions of the small rectangular region outlined in white in Figure 2a. Here the positions of selected slicks within the earlier forward view are traced in red. The downstream (roughly northeastward) spatial displacement of the small blob in the nadir inset of Figure 2b is 32.5 m, which corresponds to a surface current of  $0.72 \text{ m s}^{-1}$ . In this basic

investigation of the performance of the ATSSG technique, we have not yet made use of pattern recognition techniques in determining differential displacements. Furthermore, for these calm conditions we have assumed that the slicks undergo relatively little deformation over the (45.3 s) time interval separating the paired images. A detailed comparison of slick shapes in both the forward and nadir views sometimes reveals a pixel-scale “smudging” of features particularly in the later (nadir) image, which may reflect shape evolution due to dynamical effects [e.g., *Weber*, 2001; *Christensen and Terrile*, 2009] and/or the effects of the changing view geometry. The view-angle dependence is of particular importance with regard to inter-image comparability and in other situations may lead to the “brightness reversal” phenomenon [*Matthews et al.*, 2004; *Matthews*, 2005; *Matthews et al.*, 2008]. But we have considered only closely matching slick features in this synoptic analysis. The question of whether inter-image feature congruence holds under a wider range of wind and wave conditions warrants further investigation.

### 3. Results

[12] Selected ATSSG surface current determinations made throughout the region of interest are displayed in Figure 2c. A coherent, largely northeastward motion at speeds of typically  $1 \text{ m s}^{-1}$  is present in the main channel, whereas the pattern is confused in shallower water around Iki Island, where the presence of many small islands produces a complex flow regime. Most of the missing ATSSG coverage immediately to the north of Iki was caused by the presence of cloud. In contrast to the regular (hourly) current mapping made on a fixed grid of beam intersection points by the HF radars, the use of slicks as passive tracers of the motion means that the spatial resolution of ATSSG current mapping is variable and dependent on the distribution of surface films at the time of the satellite overpass. As a result, the ATSSG method has great potential for mapping in coastal regions where slicks are often found in profusion.

[13] Figure 2d provides the key comparison between the ATSSG surface motion determinations and the currents derived from the HF radars. The latter form two groups – those nearest to Tsushima Island in the northwest of the region covered by PRISM were observed by the NJRC radars at a working frequency of 24.5 MHz (Bragg wavelength near 6 m) and represent flows averaged within roughly the top 1 m of the water column. Further south, and closer to Iki Island and Kyushu, the current vectors were observed by the CODAR systems operating at 13.9 MHz (Bragg wavelength near 11 m) and represent motions averaged within about the top 2 m of the water column. Within the main channel, Figure 2d shows that the ATSSG flow determinations are largely consistent with the HF radar data, while the inset of Figure 2e quantifies this impression on the basis of two complex Principal Component Analyses (PCAs) in which ATSSG velocities determined within the areas covered by the two HF radars are matched with corresponding CODAR (or NJRC) velocities obtained by interpolating data from the radar beam intersections to the location of the ATSSG measurement. Each velocity is expressed as a complex number so that separate complex PCAs can then be performed for the paired data within the CODAR and NJRC regions respectively. In Figure 2e only the first PCA modes are shown,

since these explain more than 96% of the variance in both cases. Furthermore, the first ATSSG modes derived for these two areas have been scaled to ensure that their magnitudes and directions correspond to those of the overall mean ATSSG velocity. We note that in current direction there is good agreement (within  $5^\circ$  in both cases), although in amplitude (i.e. speed) differences are apparent.

[14] An alternative method of comparing these data is by simple averaging. The average amplitude (with standard deviation) for ATSSG currents in the northern comparison region is  $0.67 \pm 0.20 \text{ m s}^{-1}$ , while for the NJRC radar data it is  $0.55 \pm 0.16 \text{ m s}^{-1}$ . In the southern comparison region, the ATSSG mean amplitude is  $0.73 \pm 0.28 \text{ m s}^{-1}$  while that for the CODAR data is  $0.52 \pm 0.18 \text{ m s}^{-1}$ . A parallel comparison within the limited region in which the two radar systems overlap in coverage showed that the NJRC radar (1-m averaging depth) was measuring speeds that were typically 12% larger than those returned by the CODAR radar (2-m averaging depth). Some of the differences revealed early in the study were of an instrumental origin, such as reduced performance of one of the CODARs working near the limit of its range. However, we have now compensated for this latter deterioration by using the knowledge built up through our inter-sensor comparison. There are also differences in the spatial and temporal aspects of the respective data sampling. The ATSSG current map essentially represents a “snapshot” view of the vector motions of individual Sun glitter features recorded at the time of the satellite overpass (11.11 LT on 13 August 2006). In contrast, the NJRC and CODAR data represent averages in both time (over 10.45–11.15 LT and 10.30–11.30 LT respectively) and in space (over cells that are typically around  $10 \text{ km}^2$  in area as determined by the configuration of the beam intersection points).

[15] In addition to these instrumental and sampling issues, a number of fundamental questions arise in relation to the different aspects of the surface flow regime sensed by the ATSSG and HF radar techniques. Firstly we note that the surface films making up these slicks are not large dense agglomerates so that, as the fine-scale wave imaging in the PRISM Sun glitter data suggests, the small slicks we consider do not significantly dampen the wave field. Rather, for such moribund and well-dispersed slick features, the ATSSG technique should yield Lagrangian surface displacements that well represent the underlying “body” motion together with the full effects of wind- and wave-related forcing. In contrast, each HF radar returns a Lagrangian current which *Ardhuin et al.* [2009] decomposed into the sum of a “quasi-Eulerian” current (weighted by the Stokes drift profile of the Bragg waves) and a partial, “filtered” Stokes drift term that represents the effects of waves with frequencies up to the Bragg frequency. In theoretical studies of surface waves, the Stokes drift relevant to ATSSG data has been considered through the wave pseudo-momentum per unit mass [*Andrews and McIntyre*, 1978], or more recently the quasi-Stokes velocity [*Aiki and Greatbatch*, 2012]. These three quantities become identical when wave motions are horizontally homogeneous and irrotational in the vertical plane.

[16] In order to extend our data comparison to discuss these more subtle aspects, the ATSSG and HF radar surface current determinations made at the ADCP mooring site depicted in Figure 1 have been used to generate an approximate vertical profile for the downwind drift as shown in Figure 3 (note that the equivalent crosswind profile is not

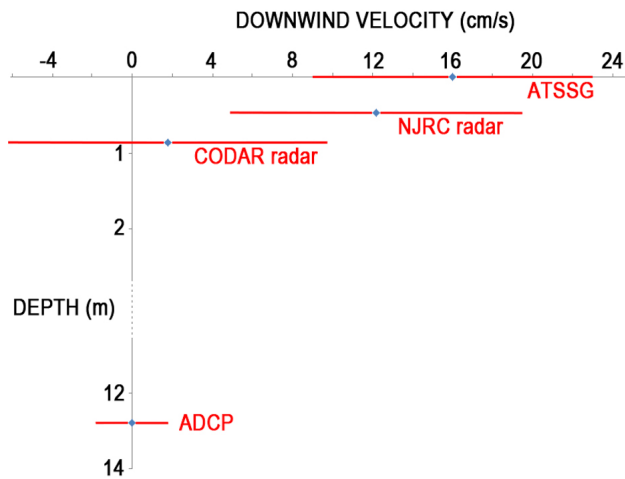


**Figure 3.** Vertical profile of downwind Stokes drift estimates made at the ADCP mooring location (defined in Figure 1). Here the ADCP data from the bin at 12.8m depth were used to remove the tidal and geostrophic flow contributions, while the template data for low wind conditions provided by *Arduin et al.* [2009] were used to remove the “quasi-Eulerian” contribution. The CODAR data were adjusted to compensate for a far-range deterioration in performance.

shown owing to the larger relative errors accruing in this direction). The ATSSG data point in Figure 3 represents the average of some 30 surface current determinations made within the vicinity (<2 km) of the ADCP mooring. We adopted an averaging approach in this specific case since no well-defined Sun glitter feature was identified directly over the ADCP mooring itself and because the slick features present in this vicinity were not so well defined. For the HF radar surface currents measured near the ADCP mooring location, we note that these remained relatively stable during the sampling time windows and that the corresponding drift values have been plotted at the center depth of the averaging layer. The current measured by the uppermost ADCP bin (at 12.8 m depth) has been used to represent the combined tidal and geostrophic flow and thus has been subtracted from both the ATSSG and the two HF radar current values. A relatively small “quasi-Eulerian” term (of  $1 \text{ cm s}^{-1}$  magnitude, downwind) was estimated for the stratified low-wind case from the template data given in *Arduin et al.* [2009]. This was simply assumed to vary little with depth near the surface and was likewise subtracted from the ATSSG and HF radar terms. The remaining downwind current components then provide a vertical drift profile that should in principle reflect the vertical variation of the Stokes drift. However, we again stress the fact that Figure 3 presents data derived from diverse current-measuring techniques each of which introduces its own characteristic error sources and spatio-temporal sampling regime.

[17] The error bar for the ATSSG downwind drift determination shown in Figure 3 mostly reflects the uncertainty associated with the geometric co-registration between image pairs, but this is augmented by smaller contributions arising from feature matching error and from the rather limited spatial variation of surface current across the 2-km averaging domain. On the other hand, the error bars shown for the NJRC and CODAR downwind drift terms were determined on the basis of extensive earlier research [*Yoshikawa et al.*,

2006], which included both inter-radar comparisons using transmissions from opposing directions along the same line of sight and detailed assessment against ADCP observations, while the error bar depicted for the ADCP downwind drift value reflects the performance specifications supplied by the manufacturer. In spite of these relatively large error bars and the gap in depth coverage between the CODAR and ADCP measurements, Figure 3 nevertheless provides an upper layer (<2 m) drift profile at a resolution not heretofore available for the open ocean. It suggests an exponential decrease in the drift with depth with an e-folding depth of less than 2 m, which is similar to the Stokes-drift profile one may expect from the wave field of roughly 10-m wavelength that is visible in the PRISM data, and assuming low wave amplitudes (<0.5 m) under the prevailing light winds.

[18] A wider aim of this assessment of the ATSSG technique was to stimulate new investigations at fine spatial detail of the type illustrated by Figure 4, which gives a comprehensive view of frontal surface current morphology that, as far as we are aware, cannot presently be obtained in any other way. This case study highlights a small coastal front that develops as waters converge at the southern end of Iki Island and appears as a well-defined summer feature in springs thermal infrared imagery (Figure 4a). Abrupt changes in the reflected Sun glitter radiance were recorded across this front in the PRISM Sun glitter data (Figures 4b, 4c, and 4d) gathered on 13 August 2006. With numerous slicks present on both sides of the front, the ATSSG technique provides a synoptic view of surface current structure in the frontal region. Even a cursory visual inspection of these data indicates strong current convergence in the region of the small red circle of Figure 4a, where surface slicks are consumed at the leading edge of the front (Figures 4b and 4c). The ATSSG mapping in the blue circle of Figure 4a shows that the head-on convergence taking place further west has now evolved into a region of well-defined current shear (Figure 4d). As surface gravity waves cross the front here they encounter an opposing current and undergo abrupt refraction. The observed direction change, of roughly  $50^\circ$ , is in line with an estimate derived from standard theory [*Kenyon, 1971*] using the ATSSG current values.

#### 4. Final Remarks

[19] The basic compatibility shown here between the ATSSG and HF radar data in both synoptic horizontal mapping and in vertical profiling at a single location provides preliminary validity support for the ATSSG technique as a means of aquatic remote sensing at high spatial resolution and demonstrates that ATSSG data can be integrated into a wider framework established on the basis of the HF radar and ADCP observations. Our study gives a good indication of the further improvements required in the performance of both the optical and radar methods of flow detection employed here. More extensive data at higher accuracy would offer a sharper insight into the influences of the various temporal and spatial sampling regimes adopted for these instrumental techniques and would highlight differences arising from the characteristics of the respective flow measurements themselves. This would in turn facilitate stricter inter-comparisons and hence support more penetrative investigations of the surface dynamics relevant to Stokes drift.

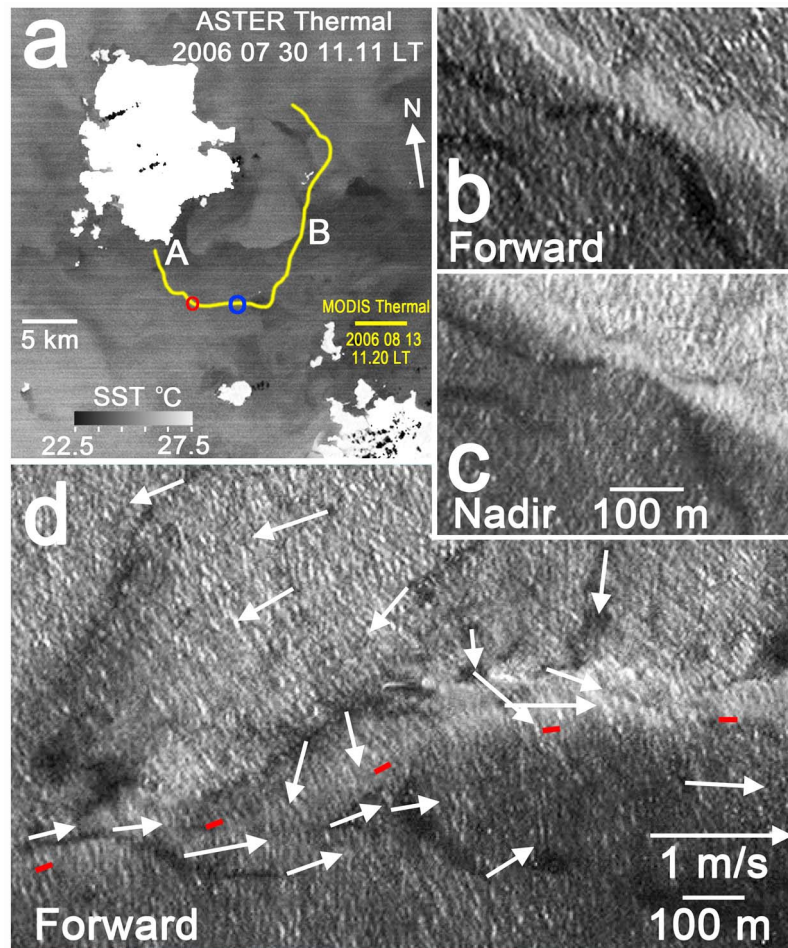


**Figure 4.** (a) ASTER Thermal Infrared image from 30 July 2006 showing the Iki coastal front as a greyscale change by  $\sim 1.5^{\circ}\text{C}$  extending between A and B. Yellow line gives the frontal position on 13 August 2006 as derived from a clouded MODIS scene, red circle indicates area covered in Figures 4b and 4c, blue circle indicates area covered in Fig. 4d. (b and c) PRISM forward and nadir views show a slick being consumed at the frontal boundary. The nadir view is obtained 45.2 s later than the forward view. (d) Detailed ATSSG mapping across the front shows surface current reversal with abrupt wave refraction. The red dashes indicate the approximate line of the leading edge of the front.

[20] Since the ATSSG technique requires daylight and cloud-free conditions and is usefully applied under low to moderate wind conditions, it is best viewed as a powerful means of promoting oceanographic process studies (of aspects such as surface dynamics, frontal research, internal and surface gravity wave propagation and slick dispersal) rather than as the main workhorse in a dedicated satellite mission to measure surface currents at high spatial resolution. At present, the latter role seems likely to be filled by all-weather, day-night operating microwave sensors such as SAR. However a validated ATSSG sensor would offer, in addition to its standalone capability, a potential means of onboard comparison or even validation for SAR-derived currents if the observational geometries adopted for these closely related optical and radar techniques could permit image acquisition in nearby or overlapping footprints.

[21] **Acknowledgments.** JPM wishes to acknowledge essential support from the Japan Society for the Promotion of Science (JSPS) and from Kyushu University, Japan. The authors also acknowledge the work of the Japan Aerospace Exploration Agency (JAXA) and the U. S. National Aeronautics and Space Administration (NASA) in developing the ASTER, PRISM and MODIS sensors. PRISM images were obtained from the

Remote Sensing and Technology Center (RESTEC) of Japan, while ASTER data were obtained from the Japanese Earth Remote Sensing and Data Acquisition Center (ERSDAC).

[22] The Editor thanks two anonymous reviewers for their assistance evaluating this manuscript.

## References

- Aiki, H., and R. J. Greatbatch (2012), Thickness-weighted mean theory for the effect of surface gravity waves on mean flows in the upper ocean, *J. Phys. Oceanogr.*, *42*, 725–747, doi:10.1175/JPO-D-11-095.1.
- Andrews, D. G., and M. E. McIntyre (1978), An exact theory of nonlinear waves on a Lagrangian-mean flow, *J. Fluid Mech.*, *89*(4), 609–646, doi:10.1017/S0022112078002773.
- Ardhuin, F., L. Marié, N. Rascle, P. Forget, and A. Roland (2009), Observation and estimation of Lagrangian, Stokes and Eulerian currents induced by wind and waves at the sea surface, *J. Phys. Oceanogr.*, *39*, 2820–2838, doi:10.1175/2009JPO4169.1.
- Bingham, R. J., P. Knudsen, O. Andersen, and R. Pail (2011), An initial estimate of the North Atlantic steady-state geostrophic circulation from GOCE, *Geophys. Res. Lett.*, *38*, L01606, doi:10.1029/2010GL045633.
- Chapron, B., F. Collard, and F. Ardhuin (2005), Direct measurements of ocean surface velocity from space: Interpretation and validation, *J. Geophys. Res.*, *110*, C07008, doi:10.1029/2004JC002809.
- Christensen, K. H., and E. Terrile (2009), Drift and deformation of oil slicks due to surface waves, *J. Fluid Mech.*, *620*, 313–332, doi:10.1017/S0022112008004606.

- Fu, L.-L., D. B. Chelton, P.-Y. Le Traon, and R. Morrow (2010), Eddy dynamics from satellite altimetry, *Oceanography*, 23(4), 14–25, doi:10.5670/oceanog.2010.02.
- Goldstein, R. M., and H. A. Zebker (1987), Interferometric radar measurement of ocean surface currents, *Nature*, 328, 707–709, doi:10.1038/328707a0.
- Goldstein, R. M., R. Li, J. A. Smith, R. Pinkel, and T. P. Barnett (1994), Remote sensing of ocean waves: The Surface Wave Process Program experiment, *J. Geophys. Res.*, 99, 7945–7950, doi:10.1029/93JC03332.
- Graber, H. C., D. R. Thompson, and R. E. Carande (1996), Ocean surface features and currents measured with synthetic aperture radar and HF radar, *J. Geophys. Res.*, 101, 25,813–25,832, doi:10.1029/96JC02241.
- Kääb, A., and T. Prowse (2011), Cold-regions river flow observed from space, *Geophys. Res. Lett.*, 38, L08403, doi:10.1029/2011GL047022.
- Kenyon, K. E. (1971), Wave refraction in ocean currents, *Deep Sea Res.*, 18(10), 1023–1034.
- Kim, S. Y., et al. (2011), Mapping the U.S. West Coast surface circulation: A multiyear analysis of high-frequency radar observations, *J. Geophys. Res.*, 116, C03011, doi:10.1029/2010JC006669.
- Liu, A. K., and M.-K. Hsu (2009), Deriving ocean surface drift using multiple SAR sensors, *Remote Sens.*, 1, 266–277, doi:10.3390/rs1030266.
- Matthews, J. P. (2005), Stereo observations of lakes and coastal zones using ASTER imagery, *Remote Sens. Environ.*, 99, 16–30, doi:10.1016/j.rse.2005.04.029.
- Matthews, D. K., and W. J. Emery (2009), Velocity observations of the California Current derived from satellite imagery, *J. Geophys. Res.*, 114, C08001, doi:10.1029/2008JC005029.
- Matthews, J. P., and T. Awaji (2010), Synoptic mapping of internal-wave motions and surface currents near the Lombok Strait using the along-track stereo Sun glitter technique, *Remote Sens. Environ.*, 114, 1765–1776, doi:10.1016/j.rse.2010.03.007.
- Matthews, J. P., A. D. Fox, and D. Prandle (1993), Radar observation of an along-front jet and transverse flow convergence associated with a North Sea front, *Cont. Shelf Res.*, 13(1), 109–130, doi:10.1016/0278-4343(93)90038-Y.
- Matthews, J. P., S. R. Wallis, and Y. Yamaguchi (2004), ASTER views a high altitude Tibetan lake in stereo, *Eos Trans. AGU*, 85(43), 435, doi:10.1029/2004EO430003.
- Matthews, J. P., X.-D. Yang, J. Shen, and T. Awaji (2008), Structured Sun glitter recorded in an ASTER along-track stereo image of Nam Co Lake (Tibet): An interpretation based on supercritical flow over a lake floor depression, *J. Geophys. Res.*, 113, C01019, doi:10.1029/2007JC004204.
- Munk, W., L. Armi, K. Fischer, and F. Zachariasen (2000), Spirals on the sea, *Proc. R. Soc. London A*, 456, 1217–1280, doi:10.1098/rspa.2000.0560.
- Prandle, D., and J. P. Matthews (1990), The dynamics of nearshore surface currents generated by tides, wind and horizontal density gradients, *Cont. Shelf Res.*, 10(7), 665–681, doi:10.1016/0278-4343(90)90044-M.
- Romeiser, R., J. Johannessen, B. Chapron, F. Collard, V. Kudryavtsev, H. Runge, and S. Suchandt (2010), Direct surface current field imaging from space by along-track InSAR and conventional SAR, in *Oceanography From Space, Revisited*, edited by V. Barale, J. F. R. Gower, and L. Alberotanza, pp. 73–91, Springer, Dordrecht, Netherlands, doi:10.1007/978-90-481-8681-5\_5.
- Steissberg, T. E., S. J. Hook, and S. G. Schladow (2005), Measuring surface currents in lakes with high spatial resolution thermal infrared imagery, *Geophys. Res. Lett.*, 32, L11402, doi:10.1029/2005GL022912.
- Turiel, A., J. Solé, V. Nieves, J. Ballabrera-Poy, and E. Garcia-Ladona (2008), Tracking ocean currents by singularity analysis of microwave sea surface temperature images, *Remote Sens. Environ.*, 112(5), 2246–2260, doi:10.1016/j.rse.2007.10.007.
- Weber, J. E. (2001), Virtual wave stress and mean drift in spatially damped surface waves, *J. Geophys. Res.*, 106(C6), 11,653–11,657, doi:10.1029/1999JC000035.
- Yoshikawa, Y., A. Masuda, K. Marubayashi, M. Ishibashi, and A. Okuno (2006), On the accuracy of HF radar measurement in the Tsushima Strait, *J. Geophys. Res.*, 111, C04009, doi:10.1029/2005JC003232.
- Yoshikawa, Y., A. Masuda, K. Marubayashi, and M. Ishibashi (2010), Seasonal variations of the surface currents in the Tsushima Strait, *J. Oceanogr.*, 66(2), 223–232, doi:10.1007/s10872-010-0020-1.